5

Selectivity control over the catalytic hydrogenation of 1,3-butadiene on Pt(111) and Pd(111) surfaces

We have studied the hydrogenation reaction of 1,3-butadiene on both Pt(111) and Pd(111) to determine why the selectivities to butenes observed experimentally are different. We propose that the distribution of products (60% selectivity on Pt vs. 100% selectivity on Pd) depends on the adsorption strength and the adsorption mode of 1,3-butadiene relative to butenes. In this chapter we show that the different selectivities on Pt and Pd surfaces cannot be satisfactorily explained by simply comparing the relative stabilities of the diene molecule and the monoalkene. Indeed, the same adsorption modes with close adsorption energies have been found for 1,3-butadiene and butene molecules on both metal surfaces. A possible explanation is found by investigating the hydrogenation reaction itself. It seems clear that the key to the selectivity to butene lies in the relative stabilities of radical intermediates on Pt(111) and Pd(111). On the platinum surface, the formation of radical species seems to compete with that of butenes. This could explain its poor selectivity to butenes and the formation of butane as a primary product.

This chapter is organised as follows: section 5.1 is a summary of the already published experimental and theoretical results for the selective hydrogenation of 1,3-butadiene to butene on transition metal surfaces; section 5.2 discusses the adsorption energies, adsorption modes and geometries of 1,3-butadiene and the three butene isomers; section 5.3 discusses the relative stabilities and surface structures of different intermediate species; section 5.4 briefly discusses coadsorption with hydrogen; section 5.5 develops the systematic study of the possible reaction pathways and analyses the results, and section 5.6 summarises the main conclusions.

5.1 Introduction

A good catalyst must have both high stability and high activity but its single most important attribute is selectivity. The selective hydrogenation of alkynes and dienes from streams containing chiefly alkenes, C_2, C_3 or C_4, is an important problem in the petrochemical industry. Steam cracking, catalytic cracking and coking lead to traces of alkynes and/or dienes, which have to be selectively hydrogenated into olefinic compounds before alkenes can be further processed by polymerisation or selective oxidation, etc. (see **Scheme 5.1**). In this context, the production of high purity butene (C_4H_8) streams for

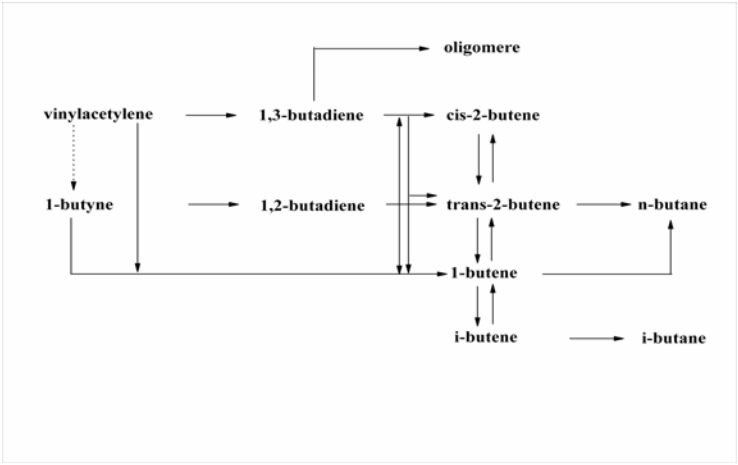

Scheme 5.1. Summary of the reactions taking place in the C_4 fraction.

polymerisation or copolymerisation processes requires the hydrogenation of the butadiene (C_4H_6) impurities contained in the butene cuts. The hydrogenation of 1,3-butadiene can lead to different products: partial hydrogenation yields to butene, while total hydrogenation leads to butane. As the target product is the alkene, the catalyst must not hydrogenate any of the butene moieties and reduce the diolefine to butene rather than butane. One should bear in mind that the traces of diene are hydrogenated in the presence of large amounts of butenes, whose conversion into butane must be kept as low as possible even when all the diene is consumed. The crucial step is then to control the selectivity of this catalytic reaction. It is generally accepted that catalytic hydrogenation processes occur by the generally accepted Horiuti-Polanyi mechanism [1,2]. Indeed, much of the research that has been devoted to acetylene and ethylene hydrogenation strongly supports this mechanism [3,4]. For the 1,3-butadiene hydrogenation, the Horuiti-Polanyi mechanism implies the initial formation of a C_4H_7 moiety and subsequent hydrogenation to a C_4H_8 species.

$$C_4H_6 \overset{+H}{\longleftrightarrow} C_4H_7 \overset{+H}{\longleftrightarrow} C_4H_8$$

Scheme 5.2

The active components of the catalysts for this reaction are usually noble metals, such as palladium or platinum. Palladium is still considered the best catalyst for the partial hydrogenation of alkadienes [5]. Exhaustive experimental studies on single crystal catalytic surfaces have shown that selectivities for the partially hydrogenated product (mainly 1-butene) approach 100% with Pd(111) while Pt(111) is much less selective (up to 60%) [6-11]. The difference between the reaction on the palladium surface and the reaction on the platinum surface was attributed to the different adsorption strengths and adsorption modes of 1,3-butadiene and butenes. It was thought that the strongly adsorbed 1,3-butadiene displaced the more weakly adsorbed butenes from the Pd(111) surface so no further hydrogenation could occur. On the other hand, the adsorption strength of 1,3-butadiene was equivalent to that of butene on the Pt(111) face. A lower selectivity was therefore expected. This hypothesis was supported by EHT calculations [12,13] and experimental studies [14,15]. However, Mittendorfer *et al.* [16] found that the adsorption energy of butadiene was stronger than 1-butene on both Pd and Pt surfaces. These authors suggested that the lower stability of 1-butene on Pd *versus* Pt could explain the higher hydrogenation selectivity observed for Pd. Unfortunately, no detailed results for the reaction mechanism are provided. Note that although much research has dealt with the adsorption of 1,3-butadiene and butene isomers on both Pt and Pd (111) surfaces, a consensus has not been reached. **Scheme 5.3** shows the different adsorption modes proposed in the scientific literature for 1,3-butadiene (CH_2=CHCH=CH_2). At low temperatures (< 95 K), 1,3-butadiene was found to be loosely bonded to both Pt and Pd surfaces [6,15]. At higher temperatures, Avery and Sheppard [17] suggested by means of EELS the presence of two adsorption modes (1,2-di-σ-adsorption and 1,2,3,4-tetra-σ-adsorption) for this molecule on Pt(111). The di-σ picture of the interaction was supported by some experimental [6,14] and theoretical [12,13] works. Bertolini *et al.* [15] reported a 1,4-di-σ-adsorbed molecule

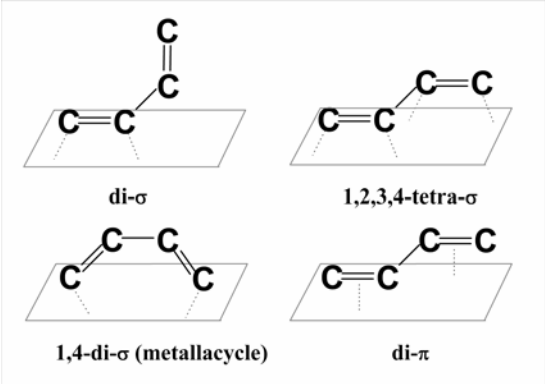

Scheme 5.3. Adsorption structures proposed for 1,3-butadiene. For sake of clarity, only C skeleton is shown.

(metallacycle). This structure was in agreement with theoretical considerations provided by qualitative molecular orbital calculations [18]. On the Pd(111) surface, UPS and NEXAFS experiments [6,15] have proposed a di-π-adsorption mode near room temperature. The picture for the various butene isomers is less ambiguous. At low temperatures, 1-butene ($CH_3CH_2CH=CH_2$) and 2-cis/trans-butenes ($CH_3CH=CHCH_3$) are di-σ-bonded to the clean Pt(111) surface, as is suggested by EELS, TDS, UPS and NEXAFS experiments [6,14,15,17,19-21]. Around room temperature, all these species desorb or transform into a more dehydrogenated molecule. On palladium, 1-butene is reported to be π-bonded at temperatures under 200 K. As on Pt(111), at higher temperatures, this molecule desorbs [6,15]. Unfortunately, to our knowledge no data are available for the 2-butene isomers adsorbed onto the Pd(111) surface. Very recent Density Functional (DF) calculations suggested that 1,2,3,4-tetra-σ for the 1,3-butadiene molecule and a di-σ adsorption mode for 1-butene are the most favoured configurations on both metal surfaces [16].

Similar thermodynamic arguments had been used to explain the high selectivity of the Pd catalyst on the hydrogenation of acetylene [2]. It was thought that the strongly adsorbed acetylene (C_2H_2) molecule displaced the more weakly bound ethylene (C_2H_4) from the Pd surface. Consequently, the surface would be predominantly covered with acetylene. The rate of acetylene hydrogenation is therefore supposed to be faster than for ethylene. However, a later study [22] indicated that these arguments are not complete because they could not explain the noticeable ethylene hydrogenation observed under high pressures of acetylene. Moreover, these classical thermodynamic arguments do not take into account the presence of other intermediate species on the surface. Vinylidene (CH_2C), vinyl (CH_2CH) and ethylidene (CH_3CH) moieties have been found to play a crucial role in ethylene formation [23].

Another interesting point in 1,3-butadiene hydrogenation is the formation of butane observed on platinum surfaces from the beginning of the reaction [24]. Butane is a primary

product of the reaction and is formed in a significant amount relative to butenes. This different behaviour was not ascribed to a very low desorption rate of the intermediate olefin but to the nature of the half hydrogenated species. Additionally, several papers dealt with the reactivity of metallacyclic intermediates that could play an important role in hydrogenation-dehydrogenation reactions [25,26,27].

In this chapter, we investigated the hydrogenation of 1,3-butadiene to several C_4H_8 species on both the Pt(111) and the Pd(111) surfaces using DFT methods. First we aimed to determine and compare the geometry, binding site preference and adsorption energies of 1,3-butadiene (C_4H_6), 1-butene and 2-*cis/trans*-butenes (C_4H_8) on both metal surfaces and discuss any general trends. Our objective was to check if simply thermodynamical arguments are enough to explain the experimental findings and evaluate the necessity of the study of the possible reaction pathways. We then further studied the hydrogenation reaction itself in order to determine the adsorption structures and relative stabilities of the various reaction intermediates (C_4H_7 and C_4H_8 radical species) and investigate the possible reaction pathways. Our results are analysed and discussed in detail.

5.2 Adsorption of 1,3-butadiene (C_4H_6) and butenes (C_4H_8) on Pt(111) and Pd(111)

5.2.1 Gas phase species

First, for the sake of comparison, we optimised the geometry of the gas phase molecules. To avoid lateral interactions between periodic images, a large box (15x15x20 $Å^3$) was taken as unit cell. The results for the 1,3-butadiene (CH_2=CHCH=CH_2, 13BD) molecule are close to those of previous experimental [28] and theoretical [29] studies. Our calculations predicted a C–C distance of 1.45 Å, a C=C of 1.34 Å and a CCC angle of ~124º for the *trans*-1,3-butadiene molecule. The values for the *cis* isomer are 1.46 Å, 1.34 Å and ~125º, respectively. For the 1-butene (CH_3CH_2CH=CH_2, 1B) and 2-*cis/trans*-butenes (CH_3CH=$CHCH_3$, 2B) the C–C distances are within 1.50-1.52 Å and the double bonds are in the interval 1.33-1.34 Å. Among the butane isomers, our calculation predicted that 2-butenes are thermodynamically more stable than 1-butene by 15 $kJmol^{-1}$.

5.2.2 Pt(111) surface

The adsorption energies of 1,3-butadiene and butanes at four different coverages are shown in **Table 5.1** for the species studied. The characteristic bond lengths for the adsorbed structures are given in **Table 5.2**. Only the 3x3 unit cell ($\theta = 1/9$) was used for all the molecules and structures. We studied the influence of the adsorbate coverage for the most stable structures and for the adsorption modes proposed in previous studies. For our purposes, we considered different unit cells: $\sqrt{3}$x$\sqrt{3}$, 2x2 and 3x2 associated with molecular coverages of 1/3, 1/4 and 1/6 ML [30]. We considered and optimised various adsorption structures. We have used the standard notation (π, di-σ…) and straightforward extensions. This notation is not directly linked to the hybridisation state of the carbon atoms but

Table 5.1. Adsorption energies ($kJmol^{-1}$) for the various chemisorption structures of 1,3-butadiene, 1-butene and 2-cis/trans-butene on Pt(111), as a function of the coverage

θ	1/3	1/4	1/6	1/9
1,3-butadiene				
di-π-cis				−114 (−13)
di-π-trans			−110(−18)	−122 (−14)
di-σ	−45(−15)	−78(−20)	−85(−14)	−89 (−10)
1,2-di-σ-3,4-π		−75(−19)	−122(−20)	−140 (−16)
1,4-di-σ-2,3-π			−137(−23)	−150 (−17)
1,2,3,4-tetra-σ			−156(−26)	−163 (−18)
1-butene				
π				−66 (−7)
di-σ	−45(−15)	−83(−21)	−91(−15)	−96(−10)
2-cis-butene				
π				−58(−6)
di-σ				−80(−9)
2-trans-butene				
π				−48 (−5)
di-σ				−81(−10)

The adsorption modes are those shown in Figures 5.1 and 5.3. The values in parenthesis are the adsorption energies per surface metal atom.

indicates how the double bonds of the molecule are bound to the surface, i.e. Pt-C bonds with the same metal atom for π and with neighbouring ones for di-σ.

We calculated the adsorption energies using the gas phase species C_4H_x (x = 6, 8) as the energy reference using the formula **2.41** (**section 2.10**, **Chapter 2**)

1,3-butadiene. The minima obtained for the 1,3-butadiene molecule are shown in **Figure 5.1**. The adsorption structures are named as di-σ (**Figure 5.1a**), di-π-*cis* (**Figure 5.1b**), di-π-*trans* (**Figure 5.1c**), 1,2-di-σ-3,4-π (**Figure 5.1d**), 1,4-di-σ-2,3-π (**Figure 5.1e**) and 1,2,3,4-tetra-σ (**Figure 5.1f**). Only in the di-σ adsorption mode is the carbon chain not parallel to the metal surface. In this mode the molecule interacts with two surface metal atoms through one of its double bonds (parallel to the surface) while the rest of the molecule is tilted away from the metal surface. The two di-π adsorption configurations are bound to the metal surface via their two C=C bonds. The nature of the molecule-surface interaction is the same in both di-π adsorption structures. The difference lies in the conformation of the adsorbed molecule (*cis* vs. *trans*). In the 1,2-di-σ-3,4-π, again the two C=C bonds are involved in the interaction with the metal surface but not in the same way. One of the double bonds interacts with two neighbouring metal atoms while the other is bound to a single surface atom. The nature of the carbon-metal interactions in the 1,4-di-σ-2,3-π is similar to the one described for the 1,2-di-σ-3,4-π adsorption mode but a redistribution of the π electron system takes place during the adsorption process. The

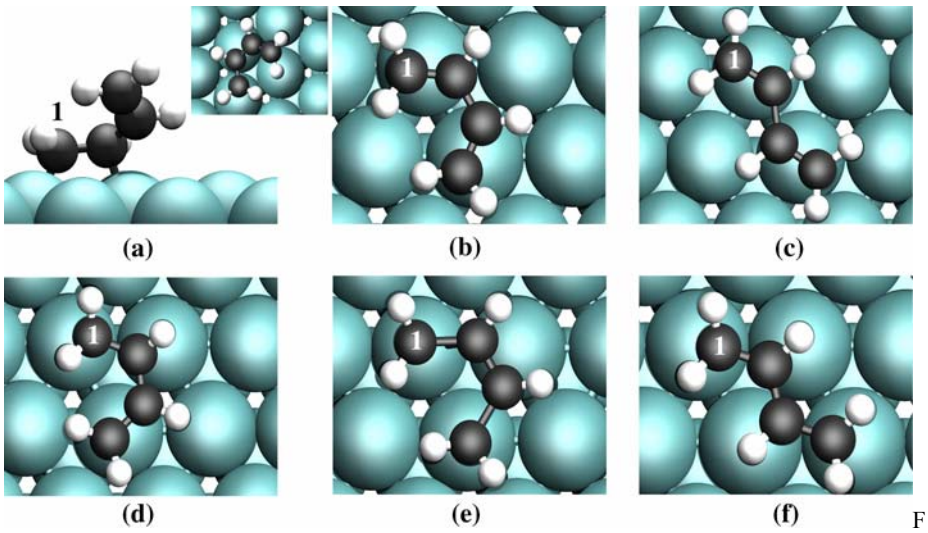

F

Figure 5.1. Adsorption modes for 1,3-butadiene on Pd and Pt (111) metal surfaces. di-σ (a), di-π-*cis* (b), di-π-*trans* (c), 1,2-di-σ-3,4-π (d), 1,4-di-σ-2,3-π (e) and 1,2,3,4-tetra-σ (f). Carbon atom number 1 is displayed for sake of clarity.

middle C–C bond gains double bond character at the expense of the terminal ones. The molecule forms two bonds through the terminal C atoms and a π-interaction via its central C–C bond. Finally, in the 1,2,3,4-tetra-σ-adsorption mode, the molecule has a *trans* conformation and interacts with the metal surface via all its C atoms.

Of all the structures tested, the most stable adsorption mode is the 1,2,3,4-tetra-σ one (**Figure 5.1f**). The 1,4-di-σ-2,3-π (**Figure 5.1e**), also called metallacycle [15,18,21], is only 13 kJmol^{-1} less stable, however. So, considering the approximations for evaluating exchange-correlation terms in GGA-DFT, the presence of a metallacycle adsorption mode on the surface cannot be excluded on the basis of total energy. The di-σ-adsorption mode is farther apart (74 kJmol^{-1}) from the most stable structure, so it can clearly be rejected. These results contradict EHT calculations made by Minot and co-workers [12] and Sautet *et al.* [13] that indicated that the di-σ adsorption mode was the most stable one on the Pt surface. Three more minima were found for the 1,3-butadiene molecule on the Pt(111) surface: the di-π, *cis* and *trans,* and the 1,2-di-σ-3,4-π adsorption modes (**Figures 5.1b**, **5.1c** and **5.1d**). The two π adsorbed modes (di-π-*cis* and di-π-*trans*) have similar adsorption energies and geometries (see **Tables 5.1** and **5.2**). These surface structures are less stable than the tetra-σ adsorption mode by 49 and 41 kJmol^{-1}, respectively. The 1,2-di-σ-3,4-π adsorption mode was only 23 kJmol^{-1} less stable than the 1,2,3,4-tetra-σ mode. Calculation of the adsorption energies per surface atom (**Table 5.1**, numbers in brackets) showed that the most stable adsorbed phase for the 1,3-butadiene at 0 K is the 1,2,3,4-tetra-σ adsorption mode in a 1/6 ML coverage. One should bear in mind that, due to steric effects, flat structures, like 1,2,3,4-tetra-σ or 1,4-di-σ-2,3-π modes, cannot exist at high coverages.

Table 5.2. Geometrical parameters for the adsorption structures of 1,3-butadiene, 1-butene and 2-cis/trans-butene on Pt(111) for a coverage of θ = 1/9 ML

	Pt–C^1	**Pt–C^2**	**Pt–C^3**	**Pt–C^4**	**C^1–C^2**	**C^2–C^3**	**C^3–C^4**
1,3-butadiene							
di-π-cis	2.17	2.25	2.23	2.17	1.42	1.47	1.42
di-π-trans	2.18	2.22	2.23	2.17	1.42	1.46	1.42
di-σ	2.11	2.17	[2.90]	[3.81]	1.49	1.47	1.35
1,2-di-σ-3,4-π	2.11	2.17	2.33	2.16	1.49	1.46	1.42
1,4-di-σ-2,3-π	2.10	2.26	2.26	2.10	1.48	1.43	1.48
1,2,3,4-tetra-σ	2.10	2.18	2.18	2.11	1.48	1.48	1.48
1-butene							
π	2.19	2.23	[2.61]	[4.01]	1.41	1.51	1.54
di-σ	2.12	2.14	[3.05]	[4.45]	1.49	1.52	1.54
2-cis-butene							
π	[3.48]	2.24	2.24	[3.44]	1.50	1.42	1.50
di-σ	[3.02]	2.15	2.15	[3.02]	1.52	1.50	1.52
2-trans-butene							
π	[3.21]	2.23	2.23	[3.24]	1.50	1.42	1.50
di-σ	[3.03]	2.13	2.13	[3.03]	1.52	1.50	1.52

Distances are in Å. The numbers in brackets account for the distance between two atoms not directly bound.

For all species studied, the Pt–C bonds are in the range 2.10-2.33 Å, which is the normal range for organometallic complexes [31]. The C–C bonds involved in the adsorption are elongated with respect to the gas phase except for the C–C central bond of the 1,4-di-σ-2,3-π structure, which gains a double bond character and is shortened during the adsorption processes. The C–C bond length is used as a measure of the activation of the adsorbed molecule. We found that the C–C bond is more elongated for the di-σ geometries than for the π ones, in relation to the stronger adsorption. The most stable structure for the 1,3-butadiene on the Pt surface expanded its C–C bonds considerably (1.48 Å). This value is close to the usual distance for a C–C single bond (1.54 Å) and is in good agreement with the C–C distance for the ethene molecule on Pt in previous experimental [32] and theoretical [33,34] studies. This indicates the σ nature of the bonding and an important reduction in the double bond character. The fact that the three C–C bonds are equal indicates that they acquire the same character upon adsorption. The σ interaction is accompanied by a rehybridisation towards sp^3 and a C–CH_2 angle of ~132º compared to 180º for an alkene, which is close to the characteristic value in alkanes (125º). On the adsorption modes named as di-π, the values of the C-CH_2 angles (~157º) are only slightly different from those of the sp^2 hybridisation.

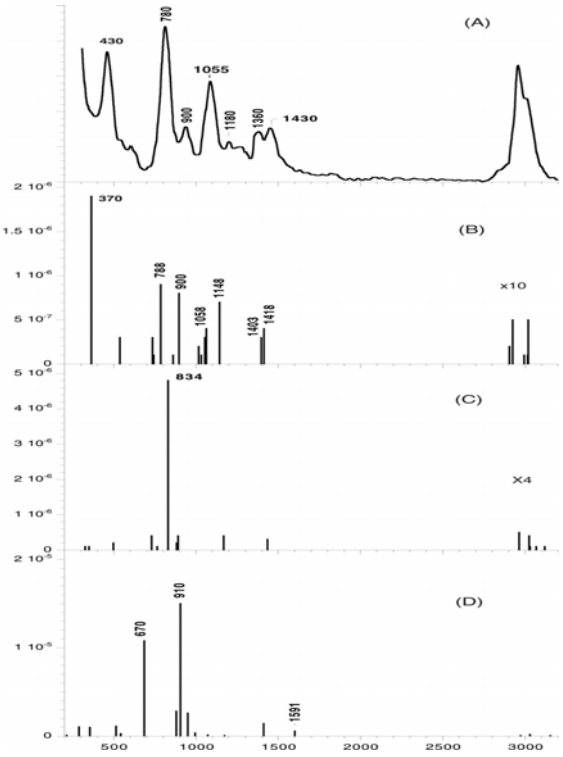

Figure 5.2. Vibrational spectra of 1,3-BD on Pt(111). Experimental EELS from ref.17 (a), 1,2,3,4-tetra-σ (b), 1,4-di-σ-2,3-π (c) and di-σ (d). Frequencies in cm^{-1}. Intensities in arbitrary units.

Since the total energy calculations did not allow a clear-cut discrimination between the two most stable structures (1,2,3,4-tetra-σ and the metallacycle), the simulation of vibrational spectra from first principles is the key to obtaining further information and direct comparisons between calculated and measured data. There is no information about coverage in the experimental sources [17,19]. We calculated the simulated spectra for the most stable system obtained in our calculations (1/6-ML). As a reference, we also calculated the frequencies of the gas phase 1,3-butadiene (see **Appendix A.4**). The good agreement between the experimental [29,35] and computed values validates the theoretical approach used to calculate the vibrational frequencies (see details of frequency calculations in **section 2.6.2, Chapter 2**). Pure DFT frequencies usually agree very well with experimental frequencies [36] but, due to anharmonic effects, C–H stretching frequencies are slightly overestimated [37,38]. The approximate description of the C–H stretching region is not a hindrance because this part of the spectrum does not hold the subsequent analysis. For our results for free 1,3-butadiene, the errors were below 2% except for the highest CH_2 as st and the lowest C=C–C bi and C–C to frequencies.

Figure 5.2 shows the experimental [17] and calculated vibrational spectra for the adsorbed 1,3-butadiene molecule. **Figures 5.2b, 5.2c** and **5.2d** correspond to 1,2,3,4-tetra-σ, metallacycle and di-σ structures respectively. The experimental EELS spectrum (**Figure 5.2a**) shows a large number of bands with intensities greater than ~1/3 of the most intense one at 780 cm^{-1}: the CH stretching bands around 2900–3000 cm^{-1} and several peaks at 1430, 1360, 1180, 1055, 900 and 430 cm^{-1}. Later HREELS studies of the same system [6,15] are comparable to this spectrum obtained by Avery and Sheppard [17].

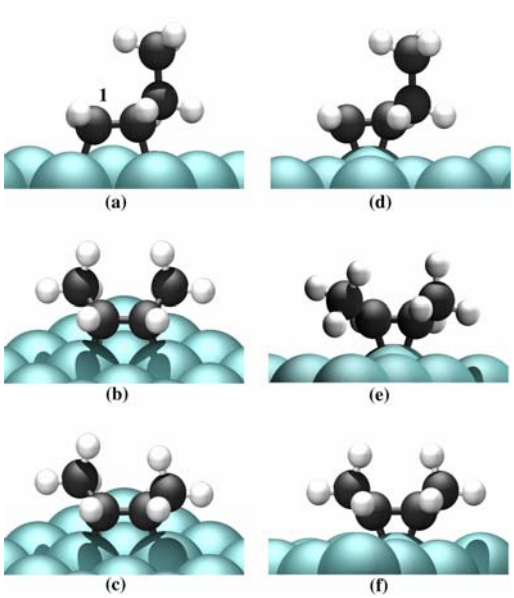

Figure 5.3. Adsorption modes for 1-butene and 2-*cis/trans*-butenes on Pd and Pt (111) metal surfaces. (a), (b) and (c) correspond to the di-σ-adsorption mode for 1-butene, 2-*cis*-butene and 2-*trans*-butene, respectively. The π-adsorption mode for the three isomers is depicted in (d), (e) and (f).

The spectrum for the tetra-σ mode (**Figure 5.2b**) matches the experimental data very well, with shifts in the calculated frequencies of 5–30 cm^{-1} and a fair agreement in the intensities. The main peaks present in the experimental spectrum also appear in the theoretical one: 1418, 1403, 1148, 1058, 900, 788 and 370 cm^{-1} assigned to the CH_2 sci (scissoring) of C^1, CH_2 sci of C^4, CH_2 ro (rocking), C=C st (stretching), CH s bo (deformation out of plane), CH_2 as to (torsion) and Pt–C totally symmetric st modes. Only the peak at 370 cm^{-1} is slightly far away from the experimental one, but this could be due to computational limitations for low frequency modes [39]. With regard to intensities, the peak at 1055 cm^{-1} (exp) is formed by the superposition of several calculated bands, and the relative calculated intensity for the main peak at 780 cm^{-1} (exp) appears to be somewhat underestimated.

The spectrum for the metallacycle adsorption mode is much less balanced and shows a dominant peak at 834 cm^{-1} assigned to the CH symmetric bending mode (out-of-plane deformation). Taking into account the finite experimental resolution, this peak may have overlapped with the band at 780 cm^{-1} (exp) and increased its intensity. However, the total absence of intense modes for this metallacycle structure around 1000 cm^{-1} and, more generally, the small relative intensity of all other peaks of the spectrum compared to the dominant one at 834 cm^{-1} indicate that this structure cannot be the majority species on the surface (see **Figure 5.2c**).

The spectrum of the di-σ adsorption mode (**Figure 5.2d**) is clearly dominated by the features at 670 and 910 cm^{-1}. Compared to these intense peaks, bands in the regions of 300, 1000 and 3000 cm^{-1} were *quasi*-negligible. For all these reasons, and due to the presence of a peak at 1591 cm^{-1} assigned to the C=C st, the agreement with the experimental spectrum is very poor. Therefore, considering the relative stabilities in the total energy calculations and comparing simulated spectra with experimental ones [6,15,17], we suggest that the 1,2,3,4-tetra-σ mode is the most probable adsorption structure. However, the metallacycle structure could be present on the surface as a minority species. This would explain why the intensity for the peak at 780 cm^{-1} is greater than that simulated for the 1,2,3,4-tetra-σ structure alone.

Butenes. For a first insight into the surface processes, we studied the adsorption of 1-butene and 2-cis/trans-butenes on the Pt(111) surface. **Table 5.1** also shows the adsorption energies for the three isomers. The picture is obviously simpler for butenes than for butadiene. Only a π or a di-σ interaction is possible for these molecules (see **Figure 5.3**). For all isomers, the di-σ adsorption mode is unambiguously the preferred one on the Pt(111) surface (the π adsorption mode was 30 $kJmol^{-1}$ less stable than the di-σ mode). We considered various conformations of the 'ethyl group' in the case of the 1-butene. Of all the possibilities we tested, the structure with the 'ethyl group' *quasi* perpendicular to the metal surface was the most stable (see **Figure 5.3a**). All the conformations where the 'ethyl' moiety was almost parallel to the surface were less stable by less than 10 $kJmol^{-1}$. If we compare the most stable adsorption mode for the three butene isomers, we find that the 1-butene is the most stable by ~15 $kJmol^{-1}$. If we consider the energy per surface unit, the 1/4-ML is the best-adsorbed phase for the 1-butene molecule on the Pt surface. The adsorption energies computed for ethylene and propylene are ~ −104 $kJmol^{-1}$ and ~ −87 $kJmol^{-1}$ (see **Chapter 4**), respectively. These values are comparable to the present results of −96 $kJmol^{-1}$ for 1-butene and −80/−81 $kJmol^{-1}$ for 2-butene. Note that the adsorption energy decreased as the number of substituents on the double bond decreased, and that propylene and 1-butene had similar values. Delbecq and Sautet [34] have shown that alkyl substituents have two effects on molecular adsorption. Their electron-donating character raises the energy of the π molecular orbitals of ethylene. The π* orbital therefore moves further away from the top of the d band, thus decreasing the back-bonding interaction and the adsorption strength. The second effect is an increase in Pauli repulsion between occupied orbitals of the molecules and the surface, which results in a larger steric effect. For 1,3-butadiene, the interaction energy is −163 $kJmol^{-1}$. This is less than twice the adsorption energy of 1-butene or ethylene. In this case, in addition to steric effects, the resonance stabilizing the gas phase butadiene lowered the binding energy. This effect has also been reported for the interaction energy of benzene on Pt(111) [40]. The computed binding energy is around −88 $kJmol^{-1}$, which is much lower than three times the adsorption energy of ethylene.

The geometrical parameters in **Table 5.2** observed the same trends as for the 1,3-butadiene molecule. The molecules interact with the metal surface through their C=C bonds, which were longer than the gas phase distance. The geometry of the chemisorbed butenes is reminiscent of the geometry of propylene adsorbed on Pt(111) (**Chapter 4**). In

Table 5.3. Adsorption energies (kJmol^{-1}) for the various chemisorbed structures of 1,3-butadiene, 1-butene and 2-cis/trans-butene on Pd(111), as a function of the coverage

θ	1/3	1/4	1/6	1/9
		1,3-butadiene		
di-π-cis				−138(−15)
di-π-trans			−123(−21)	−145(−16)
di-σ		−46(−11)		−91(−10)
1,2-di-σ-3,4-π		−53(−13)		−151(−17)
1,4-di-σ-2,3-π			−130(−22)	−154(−17)
1,2,3,4-tetra-σ			−145(−24)	−163(−18)
		1-butene		
π	−25(−8)	−41(−10)	−62(−10)	−75(−8)
di-σ	−25(−8)	−57(−14)	−70(−12)	−87(−10)
		2-cis-butene		
π				−64(−7)
di-σ				−74(−8)
		2-trans-butene		
π				−56(−6)
di-σ				−69(−8)

The adsorption modes are those shown in Figures 5.1 and 5.3. The values in parenthesis are the adsorption energies per surface metal atom.

both cases, the unsaturated C=C bond lay almost parallel to the metal surface and the alkyl groups pointed outwards from the surface.

Unlike previous studies [6-8,13-15], which have indicated that stability is similar for 1,3-butadiene and 1-butene, our calculations predicted a smaller adsorption energy for the monoalkene than for the diene molecule at low coverages (-96 vs. –163 kJmol^{-1}). At high coverages (θ > 1/4 ML), repulsive interactions between adsorbed molecules forced the diene to adopt a more 'vertical' structure. The di-σ adsorption mode is the most likely. In this case, both 1,3-butadiene and 1-butene have similar adsorption structures and very similar adsorption energies (see **Table 5.2**). Similar results have been obtained by Mittendorfer *et al.* [16] using the same method and analogous models. These authors predict a decrease of ~70 kJmol^{-1} in the energy difference between the diene and the monoalkene (-79 vs. -150 kJmol^{-1} for 1-butene and 1,3-butadiene at 1/7 ML and ~-70 kJmol^{-1} for both molecules at 1/4ML coverage).

5.2.3 Pd(111) surface

We characterised the adsorption (nature and strength) of 1,3-butadiene, 1-butene and 2-butenes on the Pd(111) surface in parallel. The adsorption structures on the Pd surface are

Table 5.4. Geometrical parameters for the adsorption structures of 1,3-butadiene, 1-butene and 2-cis/trans-butene on Pd(111) for a coverage of θ = 1/9-ML

	Pd–C^1	**Pd–C^2**	**Pd–C^3**	**Pd–C^4**	**C^1–C^2**	**C^2–C^3**	**C^3–C^4**
1,3-butadiene							
di-π-cis	2.17	2.25	2.25	2.17	1.41	1.46	1.41
di-π-trans	2.18	2.22	2.22	2.18	1.41	1.45	1.41
di-σ	2.11	2.17	[2.81]	[3.64]	1.45	1.46	1.35
1,2-di-σ-3,4-π	2.11	2.19	2.34	2.15	1.45	1.45	1.42
1,4-di-σ-2,3-π	2.11	2.26	2.26	2.11	1.45	1.43	1.45
1,2,3,4-tetra-σ	2.12	2.23	2.25	2.11	1.45	1.45	1.45
1-butene							
π	2.20	2.22	[3.20]	[4.61]	1.40	1.51	1.54
di-σ	2.13	2.14	[2.98]	[4.98]	1.45	1.52	1.54
2-cis-butene							
π	[3.29]	2.24	2.24	[3.29]	1.50	1.41	1.50
di-σ	[2.99]	2.15	2.15	[2.99]	1.51	1.46	1.51
2-trans-butene							
π	[3.09]	2.23	2.23	[3.05]	1.51	1.41	1.51
di-σ	[2.98]	2.14	2.14	[2.98]	1.52	1.46	1.52

Distances are in Å. The numbers in brackets account for the distance between two atoms not directly bound.

the same as those on Pt (see **Figure 5.1** and **5.3**). **Table 5.3** shows the adsorption energies calculated for the various molecules. We also computed the adsorption energies using the **equation 2.41**. Generally, the Pd surface clearly stabilises the π modes better than the Pt surface (the differences in adsorption energy were less than 10–25 kJmol^{-1}).

1,3-butadiene. For 1,3-butadiene, the most favoured surface structure is again the 1,2,3,4-tetra-σ adsorption mode. Surprisingly, despite the different geometrical parameters the binding energy (-163 kJmol^{-1}) is equal to the one obtained on the Pt surface. The main structural details of the adsorption structures are shown in **Table 5.4**. The diene molecule is much less distorted on the Pd(111) surface than on the Pt surface and its geometry is closer to the gas phase. The terminal C–C bonds are only elongated by 0.11 Å, and the C–CH_2 angle was ~144º. This molecule contained two activated double bonds rather than two di-σ type interactions. This illustrates that the nomenclature π and σ is not directly related to the hybridisation of the organic molecule but to the nature of the molecule-surface interaction. Such a weakly distorted tetra-σ-adsorption mode with a remaining partial π character of the molecule could explain the NEXAFS results [6,15], which were previously assigned to a di-π mode. This weaker distortion of the molecular geometry on Pd(111) than on Pt(111) has been observed in previous calculations by Sautet and co-workers for the ethylene molecule [13]. It is useful to analyse the vibrational spectrum of adsorbed alkenes to determine the

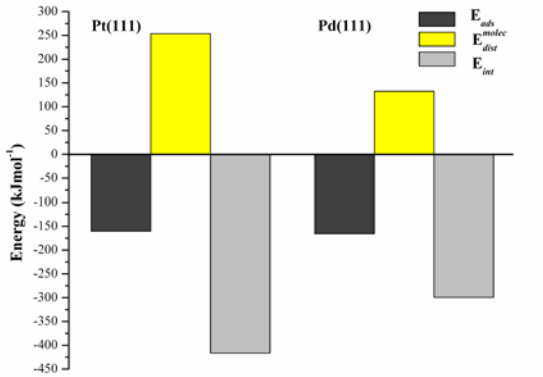

Figure 5.4. Decomposition of the adsorption energy for the most stable adsorption mode on the (111) surfaces of Cu, Pd, Pt, and Rh. Adsorption energy (dark grey), distortion energy of the molecule (yellow) and interaction energy (light grey).

state of hybridisation due to the sensitivity of the C=C stretching frequency to the hybridisation of the C atoms. In fact, in the calculated vibrational spectrum the C=C st mode appeared at 1120/1123 cm^{-1} for 1,3-butadiene adsorbed on Pd compared with 1058/1068 cm^{-1} for adsorption on Pt and 1600/1647 cm^{-1} for gaseous C_4H_6. The closer the C=C st frequency of the adsorbed molecule to the value of the gas phase, the more sp^2 hybridised the C atoms. Differences between Pt and Pd are in agreement with the periodic trends for the adsorption of ethylene on Pt-group metals [41].To explain why the adsorption strength is the same when the geometry is so different, we broke up the adsorption energy into its main components (see **Figure 5.4)**. When the molecule interacted with the metal surface, new bonds are created and the geometry of the molecule and the surface changed. The adsorption energy is therefore partitioned into the distortion energy of the molecule, the distortion energy of the surface (a minor contribution not shown in the figure) and the interaction energy between the molecule and the surface. On the Pt(111) surface, the stronger distortion of the molecule led to a higher energy cost to reach the adsorption geometry (253 $kJmol^{-1}$ on Pt compared with 132 $kJmol^{-1}$ on Pd). The molecular distortion favours the interaction between the molecule and the metal surface. If we analyse the projected density of states (PDOS, **Figure 5.5**) of 1,3-butadiene in its most favoured configuration on both metal surfaces, we can see the bonding of the π states with the metal *d*-band. The interaction mainly takes place between the p_z and the dz^2 band. The adsorbate-metal overlap is larger for Pt because the d states are more expanded (see the dotted line in **Figure 5.5**). The stabilisation due to molecule-surface interaction was greater on the Pt surface than on the Pd surface (–419 *vs.* –296 $kJmol^{-1}$). The greater elongation of the C=C bonds on Pt(111) compared to Pd(111) is clearly reflected in the PDOS. While peaks are discernible for the adsorption on Pd (arrows in **Figure 5.5**), the broadening of the corresponding states on Pt made it more difficult for peaks to be identified. As overall adsorption energy is a compromise between the distortion energy of the molecule and stabilisation due to the interaction between the molecule and the metal surface, the higher

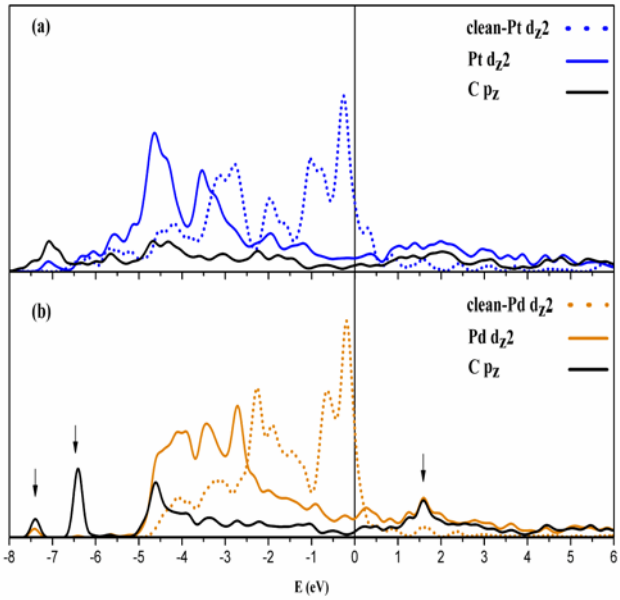

Figure 5.5. Projected density of states (PDOS) of 1,3-butadiene on Pt(111) (a) and Pd(111) (b).

energy cost needed to distort the molecule from its gas phase geometry on Pt(111) than on the Pd surface led to a similar adsorption energy on both metal surfaces. This explains why the adsorption energies of 1,3-butadiene on the Pt and Pd (111) surfaces are similar even though the adsorption geometries are quite different. Pt is clearly a case of strong interaction but also strong molecular distortion, while Pd is clearly a case of weaker interaction but with an overall adsorption that is at least as efficient.

Butenes. For all butene isomers, the preferred mode is the di-σ adsorption mode, but the difference in stability between this mode and the π mode is clearly smaller than on Pt(111) (**Table 5.3**). As with the 1,3-butadiene molecule, the adsorption geometry is closer to the gas phase than on Pt(111) and the differences between the di-σ and π adsorption geometries were clearly smaller (0.05 Å on Pd *vs*. 0.08 Å on Pt). Therefore, this moderately distorted di-σ structure on Pd kept a partial π character for the C–C bond, which is in agreement with the experimental data. These experiments have previously referred to a π adsorption mode for the molecule [6,15]. However, these results can be interpreted in a different way. Our results suggest that the molecule adsobs on the metal surface in a slightly distorted di-σ mode. We calculated the adsorption energy at different coverages for the 1-butene and 1,3-butadiene molecules. If we consider the adsorption energy per surface unit, again the preferred surface structures were the 1,2,3,4-tetra-σ adsorption mode with a coverage of 1/6-ML for the 1,3-butadiene and the di-σ mode with a coverage of 1/4-ML for the 1-butene molecule.

We need to consider two situations regarding the relative stabilities of butadiene and 1-butene. At low coverage (θ =1/9 ML), we predict a considerable difference (76 kJmol^{-1}) in the adsorption strength of the two molecules. Our calculations favour the butadiene. However, the increased coverage (θ =1/4 ML) destabilises the 1,3-butadiene molecule more than the 1-butene molecule. As observed on Pt(111), the difference in energy between these two molecules is dramatically reduced. The same findings have been previously reported by Mittendorfer *et al*. [16].

5.2.4 Pt(111) vs. Pd(111)

Although the electronic behaviour of the Pt and Pd surfaces is different, the adsorption modes are the same, with close adsorption energies for 1,3-butadiene and butenes on both metal surfaces. For the 1,3-butadiene molecule, the preferred adsorption structure is a tetra-σ mode with the four C atoms bound to four neighbouring Pt atoms. In this surface structure the carbon chain remains almost parallel to the surface. The most stable adsorption mode for the butenes is the di-σ-mode. In the optimised geometry, the C=C bond lay parallel to the metal surface and the alkyl groups pointed outwards from the surface. However, on Pd(111) the molecules are less distorted than on the Pt surface. Moreover, the π adsorption modes are less destabilised than the σ modes on Pd(111). The difference in energy between the di-σ and π modes is therefore clearly smaller on palladium. If we compare the strength of the 1-butene adsorption to that of 1,3-butadiene on the Pt and Pd surfaces, we find almost no difference. In the low coverage situation, the energy gap between the most stable adsorption modes for both molecules is 67 kJmol^{-1} on Pt(111) *vs.*76 kJmol^{-1} on Pd(111). It is therefore difficult to relate the different selectivity only to this slight tendency (only 9 kJmol^{-1}) of Pd to provide a more facile butene desorption by competition with butadiene adsorption. Indeed it is unclear why Pt could not produce the same result. If we analyse the high coverage situation, we find that adsorption energy is very similar for 1-butene and 1,3-butadiene on both metal surfaces (see **Tables 5.1** and **5.3**). The desorption of butene is therefore no longer favoured and selectivity in butenes is expected to be poor on both Pt(111) and Pd(111).

In order to complete our results, we calculated the temperature-pressure phase diagrams using the approach proposed in **section 2.9**, **Chapter 2**. At UHV conditions (P= $1\cdot10^{-13}$ Pa), the most stable surface structure for 1,3-butadiene on Pt(111) is always the 1,2,3,4-tetra-σ mode. Around 150–200 K the favoured phase corresponds to a 1/6 ML coverage (2x3 unit cell). This phase is the most stable one up to ~380 K. At this temperature, the 1/9 ML (3x3 unit cell) becomes the most favourable superstructure. Above T= 430 K no molecule remains on the surface. At reaction conditions (P= 1.10^{2} Pa), we observe the same behaviour but both the transition from the 2x3 phase to the 3x3 surface structure and the desorption take place at higher temperatures. For 1-butene adsorbed on Pt(111) the most stable adsorption mode is always the di-σ. At UHV conditions, the 1/4 ML superstructure is the most stable one up to 180 K. As the temperature increases, the 2x3 phase and the 3x3 superstructure stabilise. The temperature-pressure diagrams confirm that at a given pressure (UHV or reaction conditions from ref. [10,11]) the 1,3-butadiene is

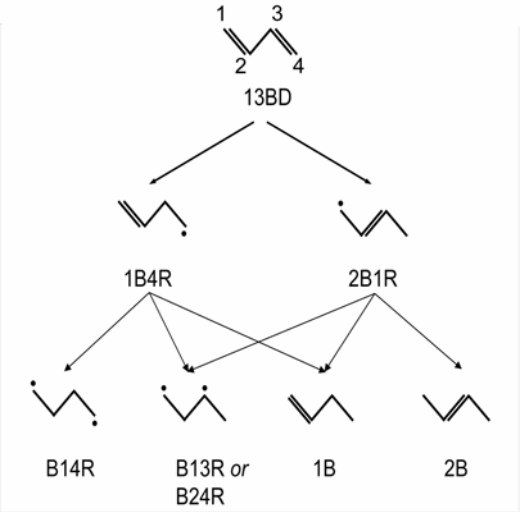

Scheme 5.4. 1,3-butadiene hydrogenation to C_4H_8 species via the Horiuti-Polanyi mechanism.

always more strongly adsorbed than 1-butene (see **Appendix A.5**). Thus, 1-butene will desorb until all the diene is not consumed.

The adsorption on the Pd(111) surface occurs in a similar way (see also **Appendix A.5**). At reaction conditions [7,9], temperature-pressure phase diagrams also predict that 1,3-butadiene more stabile than 1-butene and, consequently, a good selectivity to butenes.

To answer the problem of selectivity, it seems necessary to further study the hydrogenation reaction itself.

5.3 Hydrogenation of 1,3-butadiene on Pt(111) and Pd(111)

We carried out all the calculations presented in this section using a 3x3 unit cell (1/9 ML coverage).

5.3.1 C_4H_x (x=7, 8) radical species

Scheme 5.4 shows the network of steps by which 1,3-butadiene can be di-hydrogenated to a C_4H_8 species. We considered only the reaction pathways starting from the most stable surface structure (1,2,3,4-treta-σ). This is not a real limitation because the molecule can re-adapt its geometry before hydrogenation with the transition state research method used here [42]. The Horiuti-Polanyi mechanism (see **Scheme 5.4**) involves the

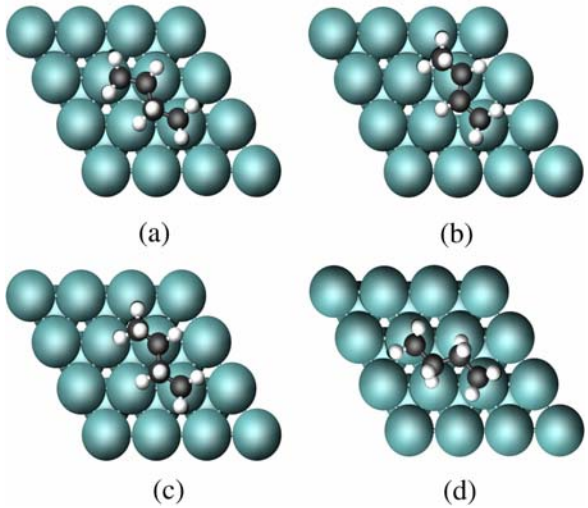

Figure 5.6. Adsorption modes for 1-buten-4-yl (1B4R, a), 2-buten-1-yl (2B1R,b), butan-1,3-diyl (B13R, c), butan-1,4-diyl (B14R, d) on Pd and Pt (111) metal surfaces.

initial formation of a C_4H_7 moiety and the subsequent hydrogenation to a C_4H_8 species. Addition of the first hydrogen atom produces only two intermediate radicals because the 1,3-butadiene molecule in the trans form belongs to the C_2h point group. The H-addition on the C^3 (or C^2) atom produces the 1-buten-4-yl (CH_2=$CHCH_2CH_2^*$, 1B4R) and the H-addition on the C^4 (or C^1) produces the 2-buten-1-yl radical (CH_2^*CH=$CHCH_3$, 2B1R). For the sake of simplicity, the nomenclature used here follows the IUPAC conventions for gas phase radicals. In the abbreviated nomenclature, the first number accounts for the position of the 'remaining' double bond and the second one account for the number of the radical C atom, R simply indicates that the fragment is a radical in the gas phase. For both radicals (1B4R and 2B1R), there are three ways to add a second hydrogen atom. For 1-buten-4-yl, the addition on C^1 produces the butan-2,4-diyl ($CH_3CH^*CH_2CH_2^*$, B24R), the addition on C^2 produces a butan-1,4-diyl radical ($CH_2^*CH_2CH_2CH_2^*$, B14R) and the addition on C^4 produces the 1-butene species. The 2-buten-1-yl radical gives 2-butene, butan-1,3-diyl ($CH_2^*CH_2CH^*CH_3$, B13R) and 1-butene from C^1, C^2 and C^3 hydrogenation, respectively. Although they are obtained in different ways, the butan-2,4-diyl and the butan-1,3-diyl species are strictly equivalent. We will name this moiety butan-1,3-diyl (B13R) in accordance with the current nomenclature.

Figure 5.6 shows the most stable adsorption modes for 1-buten-4-yl, 2-buten-1-yl, butan-1,3-diyl and butan-1,4-diyl radicals. These structures can be characterised as 1,2,4-tri-σ (**Figure 5.6a**), 1-σ-2,3-π (**Figure 5.6b**), 1,3-di-σ (**Figure 5.6c**) and 1,4-di-σ (**Figure 5.6d**). Both di-radicals form a so-called metallacycle. This adsorption structure is common for di-haloalkanes of general formula $CH_3CHX(CH_2)_nCH_2X$ (n=1,2) dissociatively adsorbed in ultrahigh vacuum [25-27]. The most important geometrical parameters and the relative adsorption energies are shown in **Table 5.5**. Obviously, a radical moiety cannot

Table 5.5. Relative adsorption energies (E_{ads} , kJmol^{-1}) and relevant geometrical parameters (metal-carbon, M-C, and carbon-carbon, C-C, distances in Å) for the different C_4H_x (x= 7–8) species adsorbed on Pt(111) and Pd(111)

molecule	E_{ads}	M–C^1	M–C^2	M–C^3	M–C^4	C^1–C^2	C^2–C^3	C^3–C^4
				Pt(111)				
1-buten-4-yl	–131	2.10	-	2.14	2.13	1.49	1.52	1.52
2-buten-1-yl	–148	2.10	2.33	2.19	-	1.46	1.42	1.50
butan-1,3-diyl	–125	2.09	-	2.12	-	1.52	1.52	1.52
butan-1,4-diyl	–80	2.11	-	-	2.11	1.53	1.54	1.53
				Pd(111)				
1-buten-4-yl	–86	2.07	-	2.15	2.14	1.45	1.52	1.52
2-buten-1-yl	–128	2.10	2.34	2.17	-	1.44	1.42	1.50
butan-1,3-diyl	–48	2.07	-	2.10	-	1.51	1.51	1.51
butan-1,4-diyl	–18	2.09	-	-	2.09	1.52	1.54	1.52

exist as such in gas phase. Adsorption energies are expressed with respect to the 1,3-butadiene molecule in the gas phase and the adsorbed hydrogen in order to compare the adsorbed species.

$$E_{ads} = (E_{C_4H_x/surface} - E_{surface} - E_{C_4H_{6(g)}}) - (x-6)(E_{H/surface} - E_{surface}) \quad (5.1)$$

Especially for butan-1,3-diyl, the Pt(111) surface stabilises the radical species more than the Pd surface, i.e. the adsorptions energies are higher on Pt(111) than on Pd. However, the trends are similar on both metal surfaces. The most stable species is the 2-buten-1-yl intermediate, followed by 1-buten-4-yl, butan-1,3-diyl and the butan-1,4-diyl radical. Note that 2-buten-1-yl is stabilised by 42 kJmol^{-1} with respect to the 1-buten-4-yl on the Pd surface while the difference is only 17 kJmol^{-1} on the Pt(111). The di-radical species are much less stable than the mono-radical moieties on Pd(111), while the difference is much smaller on the Pt(111) surface. However, we should take into account that this difference also includes the difference in the adsorption energy of the hydrogen atom on these metals (–48 kJmol^{-1} on Pt vs. –67 kJmol^{-1} on Pd). This value (~20 kJmol^{-1}) helps to explain the marked gap between C_4H_6 and the mono- and di-hydrogenated species found on Pd(111). As our aim is to study the hydrogenation of 1,3-butadiene to the different C_4H_8 species, we compare the adsorption energy of the di-radicals to that of the butene molecules (e.g. 1-butene). The relative adsorption energies for 1-butene are –136 kJmol^{-1} and –89 kJmol^{-1} on Pt(111) and Pd(111), respectively. The butan-1,3-diyl radical is only 11 kJmol^{-1} less stable than 1-butene on platinum while on palladium the difference is 40 kJmol^{-1}. The energy difference increases dramatically if we consider the 1,4-di-radical (55 kJmol^{-1} and 71 kJmol^{-1} on Pd). We will therefore not consider the butan-1,4-diyl radical in our study of the possible reaction pathways.

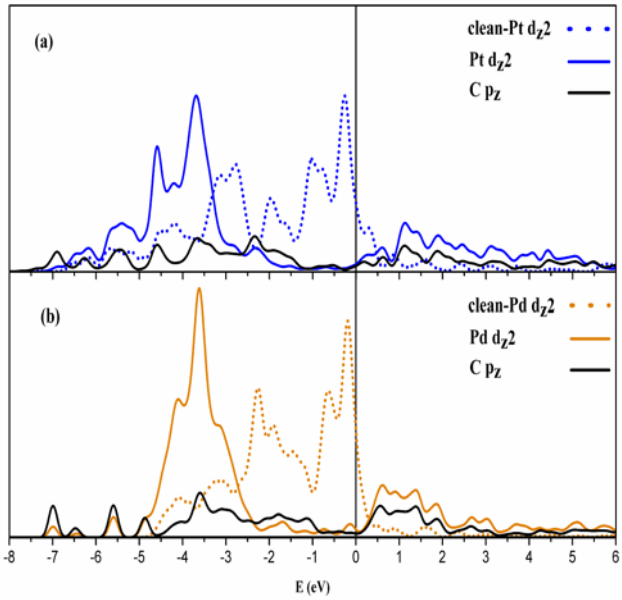

Figure 5.7. Projected Density of States (PDOS) for butan-1,3-diyl on Pt(111) (a) and Pd(111) (b).

The adsorption geometries of the radical intermediates follow the same trends as those of 1,3-butadiene and butenes. In general, there is no clear difference between the metal-carbon (M–C) and C–C bond distances of the two metal surfaces except for C–C bonds that directly interacted with the metal surface of the mono-radical species. In fact, the C^1–C^2 bond distance of the 1-buten-4-yl molecule is 1.45 Å on Pd and 1.49 Å on Pt. The same result is found for 1,3-butadiene in its di-σ adsorption mode. Moreover, the C^1–C^2 bond of the 2-buten-1-yl intermediate is also shorter on Pd than on Pt and, more importantly, the difference between the C^1–C^2 bond and the C^2–C^3 bond is smaller in Pd than in Pt which indicates a more allylic adsorption mode. Similarly, the difference in the C^1–C^2 and C^2–C^3 bond distances increases from 0.02 Å on Pd to 0.05 Å on the Pt surface for 1,3-butadiene di-σ-π adsorbed. The allylic character of the adsorption structure could be responsible for the extra stabilisation for the 2-buten-1-yl radical on Pd (see above discussion on adsorption energies). No significant differences are observed for the C–H distances (~1.10 Å). All the C–C distances in the di-radical species are within the 1.52-1.54 Å range. Clearly, all the C atoms had an sp^3 hybridisation. The C–H distances are ~1.10 Å except for the C^3–H and C^4–H bonds of the butan-1,4-radical that pointed directly to the metal surface (1.13 Å). This suggests that these bonds are slightly activated due to agostic interaction with the metal surface (the M–H distance was only about 2.12 Å).

Before continuing the study of the reaction mechanism itself, we will analyse the interaction of butan-1,3-radical and 1-butene in greater detail. The adsorption energy of the butan-1,3-diyl radical with respect to the molecule in the gas phase is –365 $kJmol^{-1}$ on

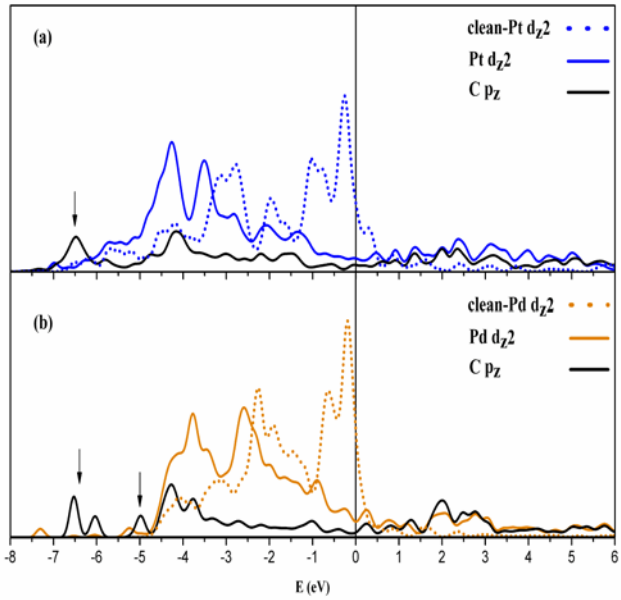

Figure 5.8. Projected Density of States (PDOS) for 1-butene on Pt(111) (a) and Pd(111) (b). Here, arrows show the peaks resulting from the interaction of the Cp_z orbital with the Md_{xz} and Md_{yz}.

Pt(111) and –327 kJmol^{-1} on Pd(111). For the 1-butene molecules it is –96 and –87 kJmol^{-1} on Pt and Pd, respectively. The di-radical species on the Pt(111) surface clearly stabilises. Comparing the projected density of states (PDOS) curves (see **Figure 5.7** and **5.8**) helps us to understand these differences. The di-radical intermediate adsorbs on both metal surfaces to form a five-atom metallacycle structure. In this adsorption mode, the carbon atom directly points to a surface metal atom. Therefore, the interacting orbitals are mainly d_z^2 for the metal atoms and p_z for the carbon. On interaction, there is a splitting of the dz^2 band (see **Figure 5.7**). The occupied part of the band is pushed downward and the empty part appears above the Fermi level (taken as zero). The d-band centre below the Fermi level is placed at –4.08 eV and –3.56 eV for platinum and palladium, respectively. Above the Fermi level, the d-band centre is located at 2.49 eV (2.17 eV) for the Pt (Pd) surface. Obviously, these values produce a larger splitting on Pt(111) (6.57 eV) than on Pd (5.73 eV). This result is consistent with the greater stability of the di-radical species on Pt(111) than on Pd(111). Two reasons can explain this difference: first, the smaller 4d orbital expansion of Pd, as seen from the narrower d-band in bulk, leads to a smaller surface-molecule overlap; second, the higher energy of the d states for Pd (more electropositive metal) increases the energy difference between them and C:p_z, which decreases the interaction.

The picture for butene species is quite similar. The interaction takes place primarily between the p_z orbital of the C atom and the d_z^2 band of the metal surface (see PDOS, **Figure 5.8**). However, there is a non-negligible contribution by d_{xz} and d_{yz} (peaks marked

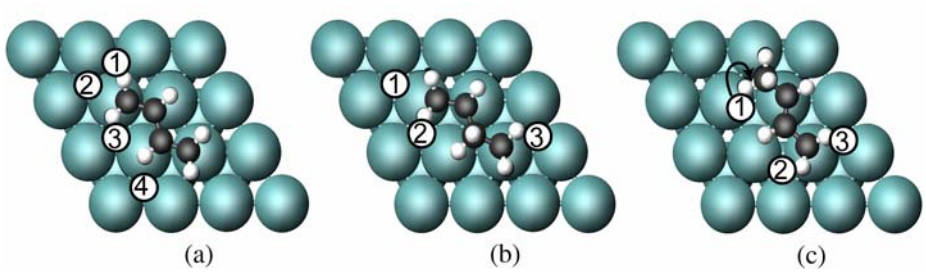

Figure 5.9. Initial hydrogen position in the co-adsorbed system. 13BD + H (a), 1B4R +H (b) and 2B1R +H (c).

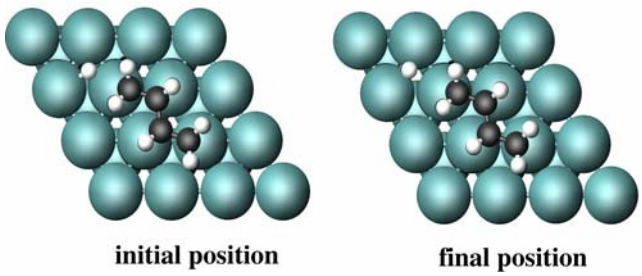

Figure 5.10. Movement of the hydrogen atom during the geometry optimisation.

with an arrow in the PDOS curves are due to these interactions, **Figure 5.8**). The C^1–C^2 bond is parallel above a metal-metal bond. This allows for a better overlap between C:pz and these bands. A considerable splitting is observed in the d_z^2 band upon adsorption of the butene molecule, though this is not as obvious as with the di-radical adsorption. Again the difference in energy between the centre of the d_z^2 band above and below the Fermi level is larger on the platinum surface (by 0.9 eV). Electronic interaction is therefore again greater on Pt than on Pd. However, the adsorption energy of 1-butene on Pt(111) and Pd(111) differed by only 9 $kJmol^{-1}$ compared with a difference of 38 $kJmol^{-1}$ for the di-radical. To explain these differences we break up the adsorption energy into its main components. These are the distortion energy of the molecule, the distortion energy of the surface and the interaction between adsorbate and substrate. For the butan-1,3-diyl radical, the difference in the distortion of the species and the surface on both metal surfaces is less than 9 $kJmol^{-1}$. The interaction energy between the di-radical and the surface is therefore higher on Pt (–434 $kJmol^{-1}$) than on Pd (–380 $kJmol^{-1}$). For 1-butene, the energy cost for distorting the molecule from its geometry in the gas phase to its adsorption geometry is 51 $kJmol^{-1}$ lower on Pd(111). The higher distortion energy on Pt is consistent with the stronger hybridisation and the greater elongation of the C_1C_2 bond on adsorption (see **Tables 5.2** and **5.5**). This is also observed in the PDOS curve (**Figure 5.8**) where the broadening of the C:pz states is greater on Pt than on Pd. As the distortion energy of the surface is similar for both surfaces, the energy interaction is 66 $kJmol^{-1}$ stronger on platinum than on palladium (–260 *vs.* –194 $kJmol^{-1}$, respectively).

5.3.2 Co-adsorption of C_4H_x (x=6,7) species and hydrogen

The next step towards understanding the hydrogenation of 1,3-butadiene was to examine the interaction between the hydrocarbon and the hydrogen atom. We calculated the co-adsorption of 1,3-butadiene, 1-buten-4-yl and 2-buten-1-yl and hydrogen for several configurations on both metal surfaces. **Figure 5.9** depicts the hydrocarbon adsorption geometries and shows the initial hydrogen positions. The C_4H_x species was placed in its more stable adsorption site and hydrogen was placed in a neighbouring 3-fold hollow site close to the C atom to be hydrogenated. On co-adsorption there are no significant changes in the geometry of the C_4H_x moiety. However, the picture for the H atom is quite different. On palladium, all the positions surrounding the organic molecule are stable. On the other hand, in the case of platinum, the hydrogen atom moves on the metal surface from the 3-fold hollow site closest to the hydrocarbon moiety (the H atom and the C_4H_x species shared at least one of the surface metal atoms) to a *quasi* bridge position (one of the metal-hydrogen bonds is elongated by about 0.15 Å) or to a neighbouring hollow site. In **Figure 5.10**, we plot the adsorption geometry for the co-adsorption of 1,3-butadiene and hydrogen on position 2, before and after the optimisation process. We can clearly see that the hydrogen atom moves towards a bridge position. In fact, the height of H above the surface is ~0.9 Å. This value is in between of those for hollow (0.8 Å) and bridge (1.0 Å) positions. This is a consequence of the well-known high mobility of H atom on both metal surfaces [43].The energy differences of the co-adsorption state with respect to the individual adsorptions of the hydrocarbon and hydrogen [44] are not negligible (around 15–30 $kJmol^{-1}$). These results are very similar to those for ethylene [23] and acetylene [45] hydrogenation.

Among the positions tested, the most stable ones were used as initial configurations for the reaction pathway searches (see **Appendix A.6**). For the sake of comparison, in the next section we provide some geometrical parameters of the co-adsorbed states.

5.3.3 Reaction pathways and activation barriers

Figure 5.11 shows the reaction profiles starting from the reactant (C_4H_6) to provide the product species (C_4H_8) on the Pt(111) surface. The reference line (zero level) is the adsorbed 1,3-butadiene and two adsorbed hydrogen atoms (without interaction). We did not consider zero point energy (ZPE) corrections to calculate the activation barriers. Some test calculations showed that the contribution of ZPE to the activation energies is less than 1 $kJmol^{-1}$ on both metal surfaces. The only noticeable effect is the destabilisation of the second hydrogenation transition states (by 30 $kJmol^{-1}$) compared to the first hydrogenation saddle points. Geometries of the transition states determined are shown in **Figure 5.12a-g**. In all cases the basic structure of the activated complex is a three-centre Pt–C–H intermediate. Whereas the C–H bond is formed, both the Pt–H and Pt–C are broken. Somehow the hydrogen atom is inserted into the C–Pt bond. Obviously, the Pt–C, C–H and

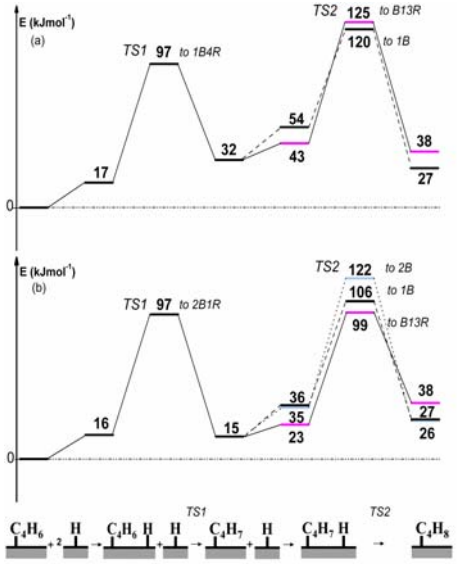

Figure 5.11. Butadiene hydrogenation energy profile on the Pt(111) surface via 1-buten-4-yl (1B4R, a) and 2-buten-1-yl (2B1R, b) intermediates. For sake of clarity, the second hydrogenation step is drawn in a different colour depending on the final product: butan-1,3-diyl radical (pink), 1-butene (black) and 2-butene (light blue).

Pt–H bond distances characterise the activated complex (see **Table 5.6**). Generally, the shorter is the C–H distance the later is the transition state.

As we explained in **section 5.3.1**, this reaction can take place via two intermediate C_4H_7 species: 1-buten-4-yl (**Figure 5.11a**) and 2-buten-1-yl (**Figure 5.11b**). For the hydrogenation of 1,3-butadiene to 1-buten-4-yl (13BD → 1B4R, see **Figure 5.12a**), as the C–H bond formed, the C–H distance decreased from 2.83 Å in the co-adsorption state to 1.65 Å. The Pt–C distance in the saddle point increased from 2.19 Å to 2.42 Å, which indicates that a clear weakening of the Pt–C bond. The computed TS energy is 97 kJmol^{-1} above the zero level, and the reaction barrier with respect to the co-adsorbed reactants (intrinsic barrier) is 80 kJmol^{-1}. For 13BD → 2B1R (see **Figure 5.12b**), the transition state is relatively early with respect to the C–H stretch (1.57 Å). Moreover, the hydrocarbon moiety remains quite flat while the hydrogen atom is inserted into the Pt–C bond. While the C–H bond forms, the Pt–C is broken (the Pt–C distance in the TS is 2.28 Å compared with 2.19 Å in the initial state). The calculated energy for the saddle point is again 97 kJmol^{-1}, with an intrinsic activation barrier of 81 kJmol^{-1}. No preference for one of the possible 'first steps' can be inferred from these results.

Table 5.6. Energy (E_{TS}, kJmol^{-1}) and the most outstanding structural parameters (metal-hydrogen, M-H, carbon-hydrogen, C-H, and metal-carbon, M-C, distances in Å) of the transition states for the 1,3-butadiene hydrogenation on Pt(111) and Pd(111)

Transition State	E_{TS}	M–H	C–H	M–C
Pt(111)				
1,3-butadiene → 1-buten-4-yl	97	1.60	1.65	2.42
1,3-butadiene → 2-buten-1-yl	97	1.61	1.57	2.28
1-buten-4-yl → butan-1,3-diyl	125	1.61	1.60	2.32
1-buten-4-yl → 1-butene	120	1.64	1.49	2.30
2-buten-1-yl → 2-butene	122	1.65	1.49	2.27
2-buten-1-yl → butan-1,3-diyl	99	1.63	1.62	3.04
2-buten-1-yl → 1-butene	106	1.93	1.42	2.46
Pd(111)				
1,3-butadiene → 1-buten-4-yl	132	1.61	1.57	2.38
1,3-butadiene → 2-buten-1-yl	96	1.73	1.50	2.31
1-buten-4-yl → butan-1,3-diyl	175	1.72	1.52	2.34
1-buten-4-yl → 1-butene	155	1.71	1.57	2.24
2-buten-1-yl → 2-butene	134	1.75	1.49	2.31
2-buten-1-yl → butan-1,3-diyl	159	1.72	1.40	3.06
2-buten-1-yl → 1-butene	120	1.81	1.46	2.36

The second hydrogenation is rather more complex. Butan-1,3-dyil and 1-butene species are obtained from the 1-buten-4-yl radical. The energy of the activated complex for 1B4R → B13R (**Figure 5.12c**) is 125 kJmol^{-1} and 82 kJmol^{-1} from the co-adsorbed state. In the Pt–C–H intermediate, the C–H distance is 1.49 Å, the Pt–H distance is 1.64 Å and the Pt–C bond length is 2.30 Å. The TS that connects 1-buten-4-yl to 1-butene (1B4R → 1B) is shown in **Figure 5.12d**. The structure is similar to that for the butan-1,3-diyl radical. Here, the C–H, Pt–H and Pt–C bond lengths are 1.49, 1.64 and 2.30 Å, respectively. The 1-butene transition state is only 5 kJmol^{-1} more stable than for the di-radical (120 *vs.* 125 kJmol^{-1}). Therefore, both reaction pathways may be competitive. The picture for the second hydrogenation from the 2-buten-1-yl radical has strong similarities with the above transition states above. From 2-butem-1-yl radical, we can obtain three different products: 2-butene, butan-1,3-diyl and 1-butene. For 2B1R → 2B (see **Figure 5.12e**), the Pt–C bond length increases from 2.11 Å to 2.27 Å while the C–H distance decreases from 2.43 to 1.49 Å. Although the TS is late with respect to the C–H stretch (1.49 Å), its adsorption site is closer to the initial sate. To reach the final state (2-butene in a di-σ adsorption mode), the molecule has to rearrange itself (the methyl group has to move upwards) and change its adsorption site (from the π to the di-σ adsorption mode). The energy of the TS is 122

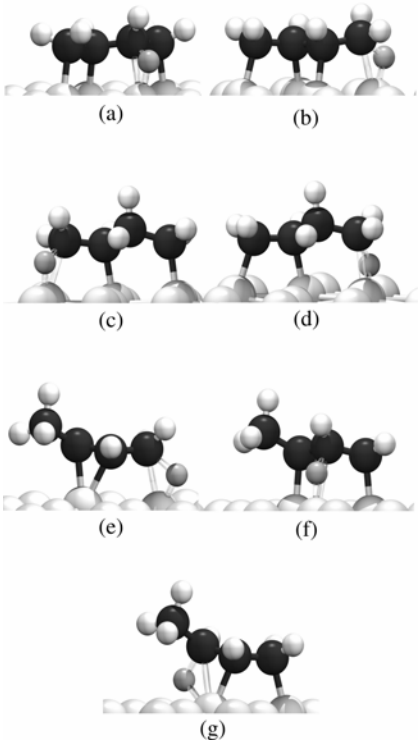

Figure 5.12. Transition state structures for the 1,3-butadiene hydrogenation on Pt(111): 13BD to 1B4R (a), 13BD to 2B1R (b), 1B4R to B13R (c), 1B4R to 1B (d), 2B1R to 2B (e), 2B1R to B13R (f), 2B1R to 1B(g). The reactive H atom is drawn in gray.

kJmol^{-1}. If we consider the barrier from the reactant state, the energy decreases to 87 kJmol^{-1}. For 2B1R → B13R (**Figure 5.12f**), the TS is near to the final adsorption site, though the C–H bond length is quite long (1.62 Å). The absolute energy of this saddle point is 99 kJmol^{-1} (intrinsic barrier: 76 kJmol^{-1}). Finally, the transition state for 2B1R → 1B (**Figure 5.12g**) is also a late saddle point. The structure of the hydrocarbon moiety is close to the final state. The Pt–C distance is 2.42 Å and the C–H is only 1.42 Å (compared to 2.17 and 2.65 Å in the initial state). The saddle point energy is 106 kJmol^{-1} above the zero level (or 70 kJmol^{-1} with respect to the co-adsorption state).

A clear trend emerges from the structure of the transition states. TS leading from a radical to a closed-shell fragment are late, with a short C–H bond (1.42–1.49 Å) and an already broken Pt–H bond (1.64–1.93 Å). The C–H bond formation process stabilises the radical fragment and overall this step is exothermic or neutral. On the other hand,

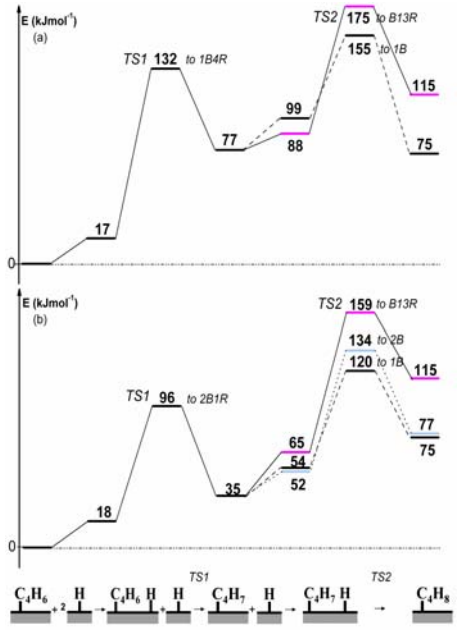

Figure 5.13. Butadiene hydrogenation energy profile on the Pd(111) surface via 1-buten-4-yl (1B4R, a) and 2-buten-1-yl (2B1R, b) intermediates. For sake of clarity, the second hydrogenation step is drawn in a different color depending on the final product: butan-1,3-diyl radical (pink), 1-butene (black) and 2-butene (light blue).

transitions from closed-shell fragments to radicals are early and endothermic, although this effect is reduced for the formation of 2-buten-1-yl since the radical is stabilised by conjugation. Radical to di-radical transition states are intermediate.

From these results we can conclude that no reaction pathway on the Pt(111) surface is favoured. The hydrogenation may take place via both the 1-buten-4-yl and the 2-buten-1-yl intermediates. Similar energies are found for all second hydrogenation transition states (the differences are less than 26 kJmol^{-1}). In the case of the pathways leading to butenes, the TS energies are consistent with a predominant formation of 1-butene (106 and 122 kJmol^{-1} for the formation of 1-butene and 2-butene, respectively). We have only calculated the pathways leading to *trans*-2-butene. Experimentally, *cis*-2-butene is obtained in almost equal quantities and the relative amount of the two isomers depends on the reaction conditions [10,11]. One could assume that the hydrogenation pathways leading to the *cis* isomer are very similar to those described above. Moreover, butene isomers are not the only surface species possible in the 1,3-butadiene hydrogenation: the butan-1,3-diyl radical is also a possibility. In fact, the saddle point leading to butan-1,3-diyl from 2-buten-1-yl (

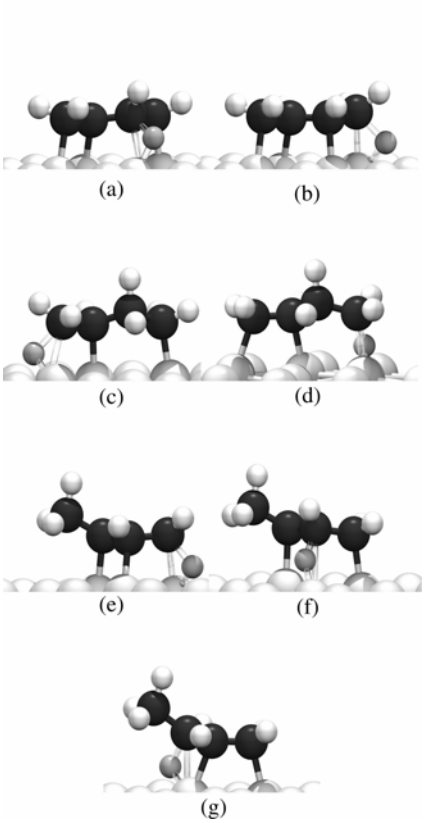

Figure 5.14. Transition state structures for the 1,3-butadiene hydrogenation on Pd(111): 13BD to 1B4R (a), 13BD to 2B1R (b), 1B4R to B13R (c), 1B4R to 1B (d), 2B1R to 2B (e), 2B1R to B13R (f), 2B1R to 1B(g). The reactive H atom is drawn in gray.

2B1R → B13R) is the most stable one (99 kJmol^{-1}). This di-radical species may continue to react, which explains the primary formation of butane observed on platinum surfaces [24].

We characterised the reaction pathways (**Figure 5.13**) on Pd(111) in parallel. The transition state structures for 1,3-butadiene hydrogenation on Pd have some strong similarities with those on the Pt surface (see **Table 5.6**), though important differences are also found. In all cases, the basic structure of the transition state is again a three-centre cyclic intermediate (Pd–C–H).

For the first hydrogenation step, the TS states to the mono-radical intermediates are similar to those for Pt(111). The hydrocarbon moiety remains flat on the metal surface and the C–H and Pd–C distances are about 1.60 and 2.30 Å, respectively (**Table 5.6**). However, the difference in energy between these two transition states is 36 kJmol^{-1} (**Figure 5.13**).

Obviously, the pathway via the 2-buten-1-yl (intrinsic barrier, 78 $kJmol^{-1}$) intermediate seems to be more favoured than the one through the 1-buten-4-yl (intrinsic barrier, 115 $kJmol^{-1}$). This important difference could be due to the poorer stability of the 1-buten-4-yl intermediate on the Pd(111) surface.

The same trends found for the first hydrogenation are also found for the second stage. The structures of the transition states are analogous to the ones obtained on Pt. There are minor differences in the C–H and M–C bond lengths i.e. under 0.1 Å (see **Table 5.6** for comparison). Only the activated complex for 2B1R → 2B is slightly shifted from its π coordination on Pt (**Figure 5.12e**) to a more di-σ co-ordination on Pd (**Figure 5.14e**). The main differences involve the saddle point energies. Clearly, the paths leading to the butene isomers (especially to 1-butene) are quite favoured on the palladium surface. The minimum energy profile occurs via the 2-buten-1-yl intermediate and leads to the 1-butene molecule. The path to the 2-butene species requires 14 $kJmol^{-1}$ more to overcome the second hydrogenation barrier. Although we may consider that hydrogenation to the *cis*-2-butene species is similar to the reaction leading to the *trans* isomer, the *trans/cis* ratio observed experimentally is quite high. The clear difference has been attributed to the low conformational interconversion of adsorbed species [9]. Both transition states leading to the butan-1,3-diyl radical are less stable than the most stable state by 39–55 $kJmol^{-1}$ (120 $kJmol^{-1}$ for the 2B1R → 1B transition state). If we take into account the possible limitations of the DFT approach, this difference is large enough to be conclusive. On the Pd(111) surface the formation of the di-radical species seems unlikely. Therefore, no alternative path to obtain butane is possible and this alkane can be obtained only by subsequent hydrogenation of butene species formed as an initial product.

5.4 Conclusions

In conclusion, we determined binding modes for 1,3-butadiene and butene isomers on Pt(111) and Pd(111). For 1,3-butadiene on Pt(111), by combining total energy calculations and simulations of the vibrational spectra, we observed that the most favoured molecular adsorption mode is 1,2,3,4-tetra-σ and reconciled the divergent proposals in the literature. On the Pd(111) surface, previuous studies suggested a di-π adsorption mode. Our calculations yielded a σ-type interaction with moderate molecular distortion, which is fully compatible with the experimental results. For butenes, our calculations indicated a di-σ adsorption mode on both metal surfaces. From experiments this has been anticipated for Pt but not for Pd, where a π mode has been predicted. As with the 1,3-butadiene molecule, the fact that molecular geometry is only slightly distorted on adsorption on Pd(111) shows that our calculations are compatible with the experimental results.

This study shows that the different selectivities for the butadiene hydrogenation on Pt(111) and Pd(111) cannot be explained only by a competition between 1,3-butadiene and 1-butene. If we compare the strength of the 1-butene adsorption to that of 1,3-butadiene on Pt and Pd, only small differences are observed. These results provided us a good starting point for the study of the reactivity.

The natural chemical pathway to hydrogenate butadiene is to conserve a double bond by forming butene (1-butene from 1-2 attack or 2-butene by 1-4 attack). The 1-3 (or 2-4) attack leads to a di-radical species, butan-1,3-diyl, which is very unstable in the gas phase. Our calculations show that this di-radical is strongly stabilised by the interaction with the catalytic surface (especially on the Pt(111) surface).

The pathway towards the butan-1,3-diyl radical becomes competitive with those leading to butenes in the case of Pt catalyst. The transformation (13BD → 2B1R → B13R) is indeed associated with the lowest activation barrier (99 $kJmol^{-1}$), but the pathway to 1-butene (13BD → 2B1R → 1B) is only 7 $kJmol^{-1}$ higher. From the typical error bars in such calculations, it is only possible to conclude here that these two pathways are equally probable. The formed butene will desorb as long as butadiene is present in the gas phase since the adsorption of butadiene is strongly favored. The di-radical species will be further hydrogenated, leading to the formation of butane as primary product and to an incomplete selectivity to butene. This is in good agreement with the partial selectivity (60%) to butene observed on Pt(111) and with the presence of butane right from the beginning of the reaction.

Although the butan-1,3-diyl is also stabilised on Pd(111), this effect is smaller than on Pt(111) and the pathway toward this radical is not accessible, with a transition state 39 $kJmol^{-1}$ less stable than that of 1-butene. Taking into account all possible sources of error, this energy difference is large enough to categorically exclude this transformation (13BD → 2B1R → B13R) on Pd(111). Calculations hence predict a full selectivity to butene in agreement with the experiment.

Moreover, the pathway to 1-butene has a lower activation energy than the one to 2-butene on both metals, in agreement with the observed distribution of products.

The smaller stabilization of the 1-3 di-radical on Pd(111) compared to Pt(111) can be qualitatively explained by the analysis of the one-electron states and related to the smaller expansion of the 4d orbitals of Pd (*vs*. 5d of Pt).

These results on the example of butadiene shed light on the factors which control activity and selectivity of a catalyst. It is well known that the key role of a catalyst is to stabilise unstable gas phase species, such as intermediates or transition states, in order to allow a lower energy profile transformation. Here, the key step is to stabilise the mono-hydrogenated intermediates 1-buten-4-yl and 2-buten-1-yl radicals. However by the same mechanism, the catalyst can also stabilise the di-radical isomers of the butene product. A selective reaction implies that the consecutive elementary steps must occur in a controlled way. Otherwise, the occurrence of side reactions leads to a poor selectivity. Therefore, an optimum catalyst for the 1,3-butadiene hydrogenation must reach a compromise between the stabilization of key intermediates and transition states and the strength of chemisorption of the unwanted di-radical intermediates.

5.5 References and Notes

[1] J. Horiuti, M. Polanyi, *Trans. Faraday Soc.* 30 (1934) 1164; J. Horiuti, M. Polanyi, *J. Mol. Catal. A Chem.* 199 (2003) 185.

[2] G.C. Bond *Catalysis by Metals*; Academic Press: London ,1962.
[3] G.C. Bond, P.B. Wells, *J. Catal*. 6 (1966) 397.
[4] J. Margitfalvi, L. Guczi, A.H. Weiss 15 (1980) React. *Kinet. Catal. Lett*. 475.
[5] Cosyns, in: *Catalyse par les Métaux*, Eds. B. Imelik, G.A. Martin, A. J. Renouprez, (Edition du CNRS, Paris, 1984) 371.
[6] G. Tourillon, A. Cassuto, Y. Jugnet, J. Massadier, J.C. Bertolini, *J. Chem. Soc. Faraday Trans*. 92 (1996) 4835.
[7] J. Massadier, J.C. Bertolini, A. Renouprez, Proc. 9th Int. Congress on Catalysis, Calgary, 1988, Eds. M.J. Phillips, M. Ternan, Vol. III, p. 1222.
[8] T. Ouchaib, J. Massadier, A. Renouprez, *J. Catal*. 119 (1989) 517.
[9] J. Goetz, D. Y. Murzin, R.A. Touroude, *Ind. Eng. Chem. Res*. 35 (1996) 703.
[10] C. Yoon, M.X. Yang, G.A. Somorjai, *Catal. Lett*. 46 (1997) 37.
[11] C-M. Pradier, E. Margot, Y. Berthier, J. Oudar, *Appl. Catal*. 43 (1988) 177.
[12] V. Maurice, C. Minot, *Langmuir* 5 (1989) 734.
[13] P. Sautet, J.-F. Paul, *Catal. Lett*. 9 (1991) 245.
[14] M. Abon, J. C. Bertolini, B. Tardy, *J. Chim. Phys.* 85 (1988) 711.
[15] J. C. Bertolini, A. Cassuto, Y. Jugnet, J. Massardier, B. Tardy, G. Tourillon, *Surf. Sci*. 349 (1996) 88.
[16] F. Mittendorfer, C. Thomazeau, P. Raybaud, H. Toulhoat, *J. Phys. Chem. B* 107 (2003) 12287.
[17] R. Avery, N. Sheppard, *Proc. R. Soc. Lond. A* 405 (1986) 27.
[18] R. C. Baetzold, *Langmuir* 3 (1987) 189.
[19] R. Avery, N. Sheppard, *Proc. R. Soc. Lond. A* 405 (1986) 1.
[20] A. Cassuto , G. Tourillon, *Surf. Sci*. 307-309 (1994) 65.
[21] Y. Tsai, B.E. Koel, *J. Phys. Chem. B* 101 (1997) 2895.
[22] W.T. McGrown, C. Kemball, D. Whan, *J. Catal.* 51 (1978) 173.
[23] M. Neurock, R. A. van Santen, *J. Phys. Chem. B* 104 (2000) 11127.
[24] J.P. Botiaux, J. Cosyns, E. Roberts, *Appl. Catal*. 35 (1987) 193.
[25] B.E. Bent, R. G. Nuzzo, B. R. Zegarski, L. H. Dubois, *J. Am. Chem. Soc.* 113(1991) 1143.
[26] T.B. Scoggins, J.M. White, *J. Phys. Chem. B* 101 (1997) 7958.
[27] D. Chrysostomou, A. Chou, F. Zaera, *J. Phys. Chem. B* 105 (2001) 5968.
[28] W. Caminati, G. Grassi, A. Bauder, *Chem. Phys. Lett*. 148 (1988) 13.
[29] G. R. De Maré, Y. N. Panchenko, J. Vander Auwera, *J. Phys. Chem. A,* 101 (1997) 3998.
[30] The 2D Brillouin integrations have been performed on a 5x5x1 grid for the √3x√3 and 2x2 structures, on a 3x5x1 grid for the 3x2 and on a 3x3x1 grid for the 3x3 unit cells.
[31] P. Ganis, I. Orabona, F. Ruffo, A. Vitagliano, *Organometallics* 17 (1998) 2646.
[32] J. Stöhr, F. Sette, A. L. Jonhnsons, *Phys. Rev. Lett*. 53 (1984) 1684.
[33] Q. Ge, D. A. King, *J. Chem. Phys*. 110 (1999) 4699.
[34] F. Delbecq, P. Sautet, *J. Catal.* 211 (2002) 398.
[35] K.W. Wiberg, R.E. Rosenberg, *J. Am. Chem. Soc*. 112 (1990) 1509.
[36] M. Saeys, M. F. Reyniers, G. B. Marin, M. Neurock, *Surf. Sci*. 513 (2002) 315.
[37] A.P. Scott, L. Radom, *J. Phys. Chem. B* 100 (1996) 16502.
[38] G. Rauhut, P. Pulay, *J. Phys. Chem.* 99 (1995) 303.
[39] Note that the coupling of the molecular vibrations and the surface phonons has been neglected
[40] C. Morin, D. Simon, P. Sautet, *J. Phys. Chem B* 107 (2003) 2995.
[41] N.F. Mrozek, M. J. Weaver, *J. Phys. Chem. B* 105 (2001) 8931.
[42] H. Jonsson, G. Mills, K. W. Jacobsen, *Nudged elastic band method for finding minimum energy path of transitions, Classical and Quantum Dynamics in condensed Phase Simulations*, J. B.

Berne, G. Ciccotti, D. F. Coker Eds, World Scientific, Singapore, 1998, 385; G. Henkelman, H. Jonsson, *J. Chem. Phys.* 111 (1999) 7010.
[43] P. Légaré, *Surf. Sci.* 559 (2004) 169.
[44] We calculated the reference energies for a 1/9 ML coverage in the same computational set up (k-points, cut-off …).
[45] P.A. Sheth, M. Neurock, C.M. Smith, *J. Phys. Chem. B* 107 (2003) 2009.